Wind Engineering Joint Usage/Research Center
FY2025 Research Result Report

Research Field: Indoor Environment
Research Year: FY2025
Research Number: 252011
Research Theme: Study on the Pollutant Exposure Reduction and Environmental Disturbance Resistance of the Neck-Side Ventilation System

Representative Researcher: Weirong ZHANG（北京工業大学）

Budget [FY2025]: 300,000 Yen

*There is no limitation of the number of pages of this report.
*Figures can be included to the report and they can also be colored.
*Submitted reports will be uploaded to the JURC Homepage.

1. Research Aim

Air Pollution Threats: Air pollutants harm millions annually; secondhand smoke, allergens, and pathogens persistently endanger respiratory health. Traditional ventilation inadequately controls exposure.

Device Limitations: N95/surgical masks cause discomfort and hinder functionality (vision, communication), with improper fit reducing efficacy. Both traditional and personalized ventilation system lack dynamic adaptability.

Wearable Tech Flaws: Head-mounted devices are bulky for daily use; face-contacting designs replicate mask discomfort.

2. Research Method

2.1 Neck-side ventilation

The neck-side ventilation strategy introduced in this work delivers clean air to the nose–mouth region through inlets placed on both sides of the neck, thereby improving respiratory protection. As it adopts a non-contact respiratory protection device (RPD), the system must rapidly supply fresh air into the breathing zone while limiting mixing with ambient flows. Air is discharged from the neck-side inlets as jets normal to the inlet plane. Owing to viscosity, these jets entrain nearby quiescent air, producing a lower pressure near the user's sides than on the opposite side. The resulting pressure gradient deflects the jets toward the face, where they attach and flow along the surface. Thus, the effectiveness of neck-side ventilation depends on identifying optimal air supply parameters that allow the jet to adhere to the face with minimal entrainment, ensuring adequate clean air around the nose and mouth.

2.2 Physical model and numerical model

To investigate the protective performance of neck-side ventilation without environmental disturbance, a 1.2 m × 1.2 m × 1 m simulation domain was created around the head and face. A mannequin representing the upper torso and head, fitted with neck-side ventilation, was placed at the center, as shown in Fig.1. Since this study

emphasizes pollutant shielding efficiency and airflow organization near the head and neck, the device was simplified to two parallel rectangular inlets on each side, spaced 140 mm apart, each measuring 110 mm × 10 mm. Two supply velocities, 2 m/s and 1 m/s, were chosen to represent high-speed and low-speed operation. This range captures relative airflow velocity differences while being appropriate for angle-dependent evaluation. The inlet pitch angle was varied at 30°, 35°, 40°, and 45°, and the airflow roll angle was adjusted at 0°, 15°, 30°, and 45°. The pitch angle selection was based on preliminary tests considering eye discomfort thresholds and protection, while the roll angle was increased from 0° until vertical and horizontal momentum components became balanced. To illustrate these variations, the angle settings were mapped onto an aircraft's three-axis model, as shown in Fig.1. Ideally, air from both inlets rises obliquely along the neck, deflects forward under the Coanda effect, and forms a protective clean-air layer in front of the nose and mouth. To simulate human thermal plumes realistically, the mannequin surface temperature was set at 35°C. Since the simplified model excluded the lower torso, it was positioned above a circular 0.5 m diameter area treated as a velocity inlet. According to Carven et al.'s thermal plume measurements, the inlet velocity was set to 0.05 m/s with a temperature of 30°C.

To assess the influence of environmental disturbances on neck-side ventilation, this study performed simulations using a full-body human model equipped with a neck-side air supply device. The model height was 1.78 m, and the outlet was simplified to two parallel rectangular openings spaced 140 mm apart, as illustrated in Fig.1. The supply angle was fixed at a pitch of 40° and a roll of 45°. For a stationary model, the neck-side supply velocity was set between 1 m/s and 3 m/s, while for a moving model, it ranged from 2 m/s to 5 m/s. These values are consistent with airflow ranges commonly adopted in wearable ventilation systems designed to enhance thermal comfort. To evaluate the effect of ambient wind, background inlets were introduced with wind speeds of 0.5 m/s, 1 m/s, and 2.5 m/s. For pollutant dispersion analysis, nitrogen (N_2) was applied as a tracer gas, with its mass fraction in the background supply air set to 0.5.

The simulations were carried out in ANSYS Fluent using a steady-state CFD method. The SST k-ω turbulence model was applied to resolve the flow field, with a near-wall y+ value close to 1, satisfying its requirements for near-wall predictions. Pressure–velocity coupling was handled through the SIMPLE algorithm. Convection and diffusion terms in the governing equations were discretized with a second-order upwind scheme. Buoyancy effects caused by body heat were represented using the Boussinesq approximation. Tracer gas concentration was calculated through the species transport model.

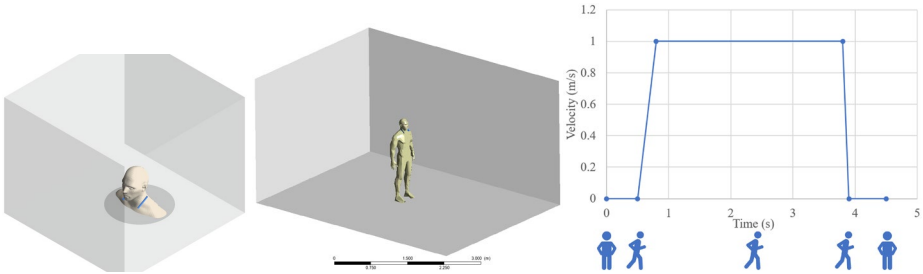

Fig. 1 Geometric model and movement speed diagram

For the selection of walking speed, we referred to the current literature on the average walking speed of indoor personnel. Tao et al. [12] found that the average walking speed of indoor personnel is usually between 0.8 and 1.2m/s. Assaad et al. investigated the impact of indoor personnel walking on personalized ventilation, setting the walking speed at 1m/s in the simulated conditions[13]. Therefore, in the absence of further evidence, we assume that 1m/s is approximately the typical average walking speed indoors and use it as a reference value for evaluating the impact of walking on personnel.

2.3 Experimental validation

The experiments were conducted in a laboratory at Beijing University of Technology, located in the basement of a building with high-quality insulation to minimize the influence of outdoor temperature on the environment. Indoor temperature was controlled within ±0.3°C. A head–neck model was adopted to represent a user of the neck-side ventilation system. The head model, based on the average male size, was hollow with an incandescent bulb inside to provide heat. A 400 mW laser installed above the setup illuminated the vertical plane of the model, while a recording device placed on the right side captured airflow visualization in 4K resolution at 30 frames per second. To reduce light reflections, a black velvet cloth was positioned on the left side of the model. An aerosol generator located in front produced aerosols from a propylene glycol and glycerol mixture to ensure operator safety. After aerosol concentration stabilized, video acquisition began. A schematic of the setup is presented in Fig.2.

The neck-side ventilation device employed in the airflow visualization tests included an air supply unit on each side. Each unit was driven by a fan equipped with two centrifugal blowers, with impeller diameters of about 45 mm. The fan provided three speed levels, of which the high and low settings were chosen for testing. To decrease airflow turbulence intensity, straws with adjustable elbow angles were evenly arranged at the reducer outlet. A schematic diagram of the fan and reducer configuration is shown in Fig.2.

After passing through the reducer and flow-straightening section, the outlet velocity was recorded as 2.04 m/s in high-speed mode and 0.98 m/s in low-speed mode using a Testo 425 hot-wire anemometer. The neck-side ventilation units were installed on both sides of

the mannequin's neck, about 3 cm away, supported by a rotating bracket with limiters that enabled adjustment of the air supply angles.

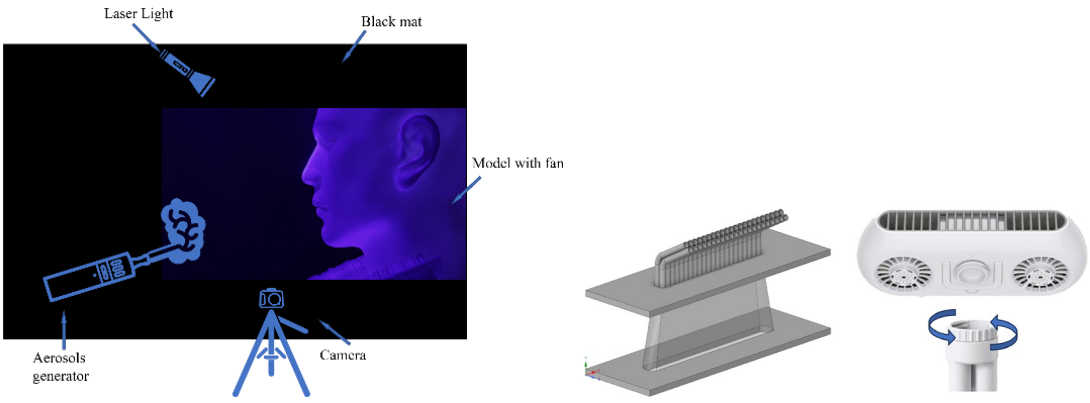

Fig.2 Schematic Diagram of the Experiment and Equipment

As illustrated in Fig.3, the aerosol distribution under three neck-side ventilation conditions is shown. In Fig.3(a), with the device turned off, aerosols move directly toward the mannequin's nose and mouth without resistance. After striking the face, they disperse outward, forming a high-concentration zone across the facial surface. The pollutant level in the main airflow region is nearly the same as that near the face, leaving sensitive areas such as the nose, mouth, and eyes fully exposed to contaminants.

In Fig.3(b), when low-speed neck-side ventilation is active, the pollutant concentration near the face is noticeably reduced. The primary aerosol stream, influenced by the ventilation jet, is deflected toward the upper left of the image before reaching the face. No sharp boundary exists between the polluted and clean air, creating a gradual diffusion zone with decreasing concentration. Although some pollutants spread toward the facial region, the concentration immediately adjacent to the face remains much lower than in the main airflow.

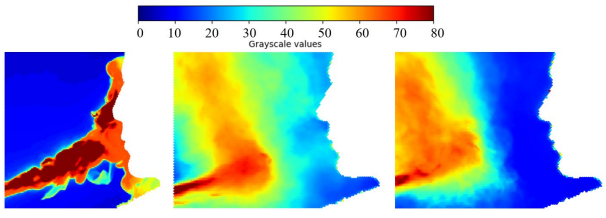

(a) Off (b) Low-Speed (c) High-Speed

Fig.3 Airflow Visualization Experiment Results

As shown in Fig.3(c), when the neck-side ventilation operates at high speed, pollutants, like in the low-speed case, are deflected toward the upper left of the image by the ventilation jet. However, unlike the low-speed condition, a distinct boundary appears between polluted and clean air. The pollutant diffusion zone is significantly compressed, and the area near the face is nearly free of contaminants, with air remaining essentially clean. Comparing the three images, it is evident that neck-side ventilation effectively

delivers relatively clean air around the nose, mouth, and adjacent facial regions.

To verify the CFD model's accuracy, steady-state simulations were performed at low airflow speed using the same boundary conditions as in the experiment applied to the geometric model. Because the image grayscale data cannot be directly compared with CFD results, normalization is required. Air within 7 cm in front of the face, corresponding to half the thickness of the head's thermal plume boundary layer, was selected. This region was divided into seven layers at 1 cm intervals, and the concentration in each layer was averaged and then normalized. The normalization procedure is presented in Equation (1),

$$C_{n,nor} = \frac{C_n - C_{min}}{C_{max} - C_{min}}, \qquad (1)$$

where $C_{n,nor}$ represents the normalized concentration of the air layer; C_n represents the average concentration or grayscale value of the air layer; C_{min} represents the minimum concentration or grayscale value within the 7 cm range in front of the face; and C_{max} represents the maximum concentration or grayscale value within the same range.

(a) Experiment result (b) CFD result

Fig.4 CFD Simulation Validation of the Airflow Visualization Experiment

The results are shown in Fig.4. It can be observed that, under the current CFD settings, the simulation results show a certain similarity to the visualization experiment. There is an acceptable level of consistency between the two results, indicating that the numerical method is reliable.

By comparing the two, we attribute the discrepancies between simulation and experiment to the relative instability and non-uniformity of aerosol generation during the experiment, in contrast to the controlled conditions of the simulation. This fluctuation, resembling a pulsed output, leads to less consistent aerosol injection and increases susceptibility to variations in the surrounding airflow.

Overall, the CFD images exhibit a satisfactory level of consistency with the experimental images, confirming that the CFD model is well-validated and that the simulation results are reliable.

3. Research Result

3.1 Effectiveness of neck-side ventilation in diffused pollutant environments

In many studies on personalized ventilation (PV), several metrics have been introduced to evaluate performance, including ventilation effectiveness (VE), inhalation fraction (IF), air quality index (AQI), personal exposure effectiveness (PEE), protection effectiveness (PE), and pollutant exposure reduction (PER). In this study, PER was selected to assess the pollutant shielding performance of the neck-side ventilation system. This metric represents

$$\mathrm{PER} = \frac{C_E - C_I}{C_E - C_P} \tag{2}$$

the proportion of treated supply airflow in the inhaled air and is calculated using Equation (2):

Where C_E represents the pollutant concentration in the ambient air, defined in this study as the average concentration within a 1m² breathing plane around the nostrils. C_I is the pollutant concentration of the inhaled air, and C_P is the pollutant concentration in the treated supply airflow, which is set to 0 in this study.

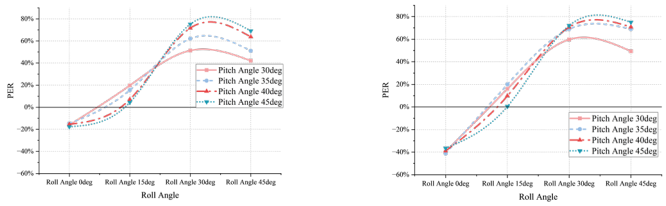

(a) 1m/s Supply air speed (b) 2m/s Supply air speed

Fig. 5 Impact of Airflow Roll Angle on PER

Fig.5(a) shows the change in PER with increasing airflow roll angle for four combinations of inlet pitch angle and ventilation speed at 1 m/s. The figure indicates that at a roll angle of 0°, PER values for all air supply conditions are negative, averaging approximately -15%. This suggests that, at this angle, operating the neck-side ventilation not only fails to reduce pollutant exposure but also increases inhalation at the nose and mouth due to entrainment and induction effects from the airflow jet.

When the airflow roll angle increases to 15°, PER values for neck-side ventilation become positive, indicating the onset of a protective effect. In this case, smaller inlet pitch angles yield higher PER values, although the overall protective effect is still limited at this stage.

As the airflow roll angle rises from 15° to 30°, PER values improve for all four pitch angles. However, larger pitch angles exhibit a more pronounced increase in protection. At a pitch angle of 45°, PER reaches about 75%. As the roll angle further increases to 45°, the protective effectiveness of neck-side ventilation declines for all four pitch angle settings.

Fig.5(b) presents PER results for 16 operating conditions at an airspeed of 2 m/s. Similar to Fig.5(a), PER is negative at a roll angle of 0°, indicating that neck-side ventilation adversely affects the nose and mouth. Comparing Fig.5(b) with Fig.5(a) shows that higher air supply speeds increase pollutant entrainment by the ventilation. A roll angle of 15° represents a clear turning point, as the ventilation begins to provide a positive effect beyond this angle. With further increases in roll angle, the protective effect becomes more pronounced. The improvement trend across pitch angles mirrors that observed at 1 m/s, with a pitch angle of 45° yielding the best protection. At a roll angle of 45°, PER values for 45°, 40°, and 35° pitch angles converge, indicating a plateau in protective effectiveness under these conditions.

Combining the observations from Fig.5(a) and Fig.5(b), when the airflow roll angle is 0°, airflow speed is the primary factor influencing PER. As the roll angle increases, the inlet pitch angle becomes the dominant factor. This indicates that the influence of airflow parameters on pollutant shielding shifts from speed to directional control with increasing roll angle.

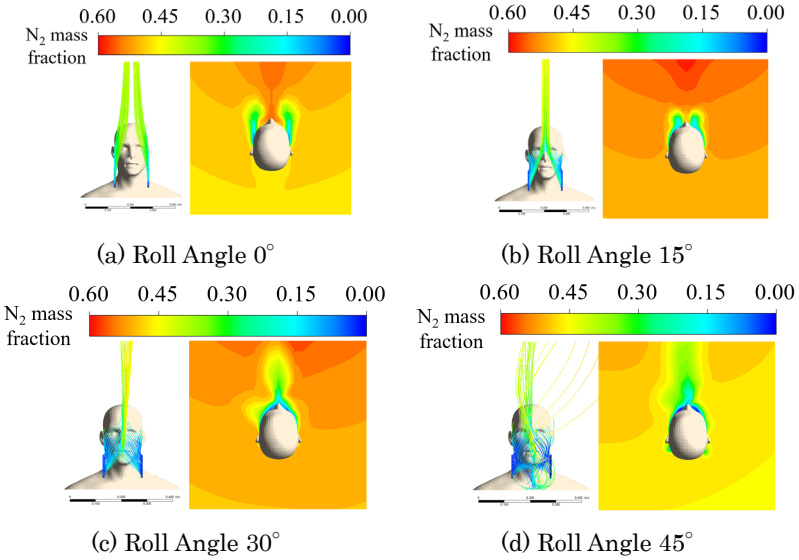

Fig.6 Streamline and Top-View Concentration Contour Maps under 2 m/s Airflow Speed and 45° Pitch Angle for Different Roll Angles

To further examine the factors affecting the influence of roll angle on neck-side ventilation, a representative case with a pitch angle of 45° and an air supply speed of 2 m/s was selected. Streamline plots of the airflow and top-view concentration contour maps were generated for analysis.

As shown in Fig.6(a), when the roll angle is 0°, the Coanda effect is weak, and the airflow only slightly deflects toward the central axis of the face. The top-view concentration contour map indicates that fresh air does not converge at the nose and mouth. Instead, a channel forms between the two high-speed clean air streams, creating an entrainment zone that draws in surrounding polluted air. This behavior is consistent with the observations in

Fig.6, where higher air speeds at a 0° roll angle worsen pollutant exposure.

As the roll angle increases to 15°, shown in Fig.6(b), the air supply jets deflect toward the nasal axis after exiting the neck-side inlets and converge in front of the nose. However, the relatively high convergence point limits the airflow's ability to provide effective protection directly around the nose and mouth.

As the roll angle increases further, shown in Fig.6(c), the clean air deflects along the cheeks and converges directly at the nose and mouth before moving obliquely upward along the face. The top-view concentration contour in Fig.6(c) shows that a clean air layer with an N_2 mass fraction below 0.12 forms around the nose and mouth, and within a certain thickness, the N_2 fraction does not exceed 0.3. This indicates that, under these ventilation conditions, an effective facial clean air layer capable of enhancing PER is established.

When the roll angle reaches 45°, shown in Fig.6(d), part of the airflow is blocked at the chin, generating a large vortex beneath this area. Nevertheless, the remaining clean airflow continues to form a thin protective layer on the face, preserving some effectiveness.

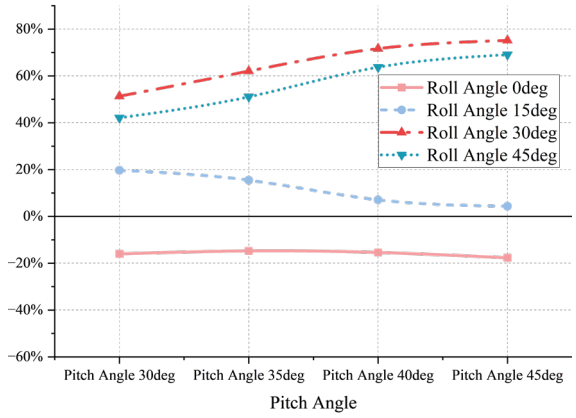

(a) 1m/s Supply air speed

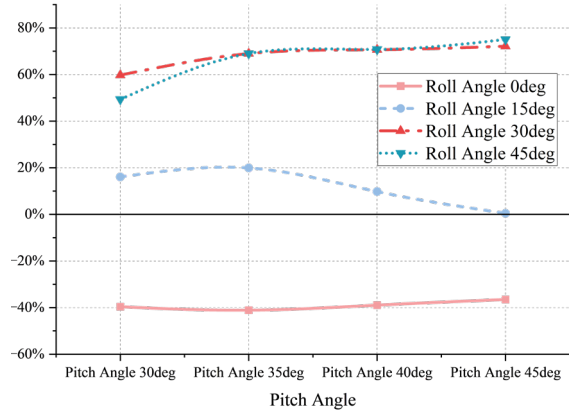

(b) 2m/s Supply air speed

Fig. 7 Impact of Inlet Pitch Angle on PER

Fig.7(a) presents PER values for 16 ventilation conditions at an airspeed of 1 m/s. The

four roll angle settings can be intuitively divided into three groups. At a roll angle of 0°, PER shows little variation with changes in pitch angle, indicating that neck-side ventilation is insensitive to pitch adjustments at this angle. However, PER values remain consistently negative, suggesting that this configuration is generally unsuitable for practical application.

When the roll angle is 15°, it forms another distinct category. Under these ventilation conditions, the PER decreases as the pitch angle increases.

Roll angles of 30° and 45° are grouped together due to their relatively high PER values, making them the recommended settings for neck-side ventilation. Under these conditions, PER increases with pitch angle. At a 30° roll angle, PER can improve by up to 23.86%, while at 45°, the improvement reaches 26.95%.

Fig.7(b) shows the effect of pitch angle on PER at an airspeed of 2 m/s. The overall trend aligns with the low-speed results in Fig.7(a). However, under these conditions, the case with a 45° roll angle demonstrates greater sensitivity to pitch angle changes, leading to relatively larger PER improvements.

A comprehensive analysis of PER variations at the two airspeeds shows that, for roll angles providing effective protection (30° and 45°), increasing the pitch angle appropriately enhances the protective performance of neck-side ventilation. For other roll angle settings, pitch angle is not a decisive factor in improving effectiveness.

3.2 Effect of neck side ventilation under environmental disturbance

3.2.1 The influence of the oncoming wind

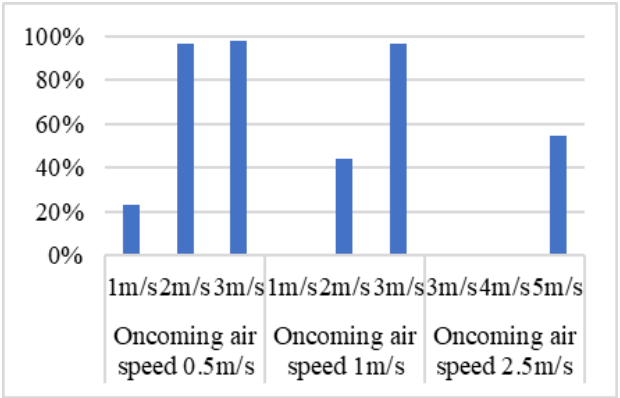

Fig.8 PER of each neck-side ventilation speed under different oncoming wind speed

Fig.8 presents PER under different neck-side supply air speeds when ambient wind blows from the front at varying velocities. For ambient wind speeds of 0.5 m/s and 1 m/s, the neck-side supply air was adjusted between 1 m/s and 3 m/s, while for an ambient wind of 2.5 m/s, the adjustment range was 3–5 m/s. When ambient wind blows toward the face at 0.5 m/s, a neck-side supply of 2 m/s achieves a high cleanliness effect, with PER reaching 96.6%. Increasing the supply speed to 3 m/s provides minimal additional benefit, with PER rising by only 1.6%. As ambient wind increases to 1 m/s, a higher neck-side supply velocity

is required for optimal protection. At 3 m/s, PER reaches 96.4%, effectively shielding most contaminants. When ambient wind reaches 2.5 m/s, even a 5 m/s neck-side supply fails to form an effective clean air layer. Further increasing supply speed is impractical, as the excessive airflow would cause an uncomfortable blowing sensation.

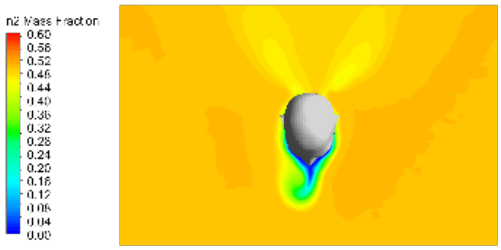

a) wind 0.5m/s-air supply 2m/s

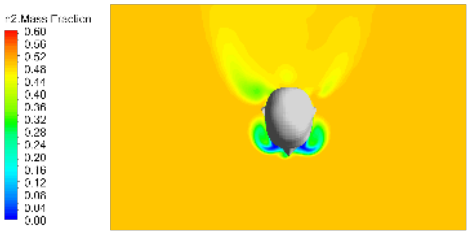

b) wind 1m/s-air supply 2m/s

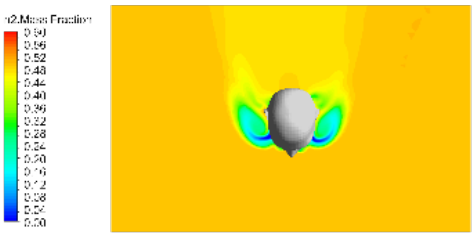

c) wind 2.5m/s-air supply 4m/s

Fig.9 Top view of the concentration cloud map under ooncoming wind

Fig.9 presents a top-down view of clean air layer formation at the height of the mouth and nose under three different ambient wind speeds. Fig.9(a) shows the facial clean layer when ambient wind is 0.5 m/s and neck-side supply air is 2 m/s. Under these conditions, airflow from the neck-side converges at the face, providing protection for the mouth and nose. As ambient wind increases, the clean airflow from the neck-side struggles to converge directly in front of the mouth and nose. Part of the airflow is deflected along the cheeks by the oncoming wind, forming a moustache-like pattern, while another portion still converges in front of the face but offers limited protection due to insufficient flow, as shown in Fig.9(b). Fig.9(c) depicts pollutant concentration when ambient wind rises to 2.5 m/s and neck-side supply air increases to 4 m/s. Even at this higher supply speed, the airflows from both sides fail to converge at the mouth and nose, providing no protective effect, which aligns with the results shown in Fig.8.

3.2.2 The influence of the movement

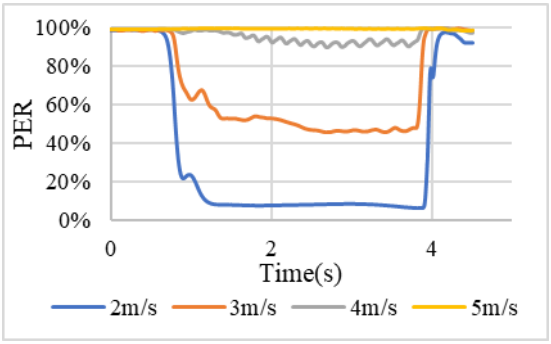

Fig.10 The PER variation of the four air supply speeds during movement

Fig.10 illustrates the changes in PER under different neck-side air supply speeds when subjected to a single disturbance caused by human walking. From an overall perspective, the neck-side ventilation undergoes four distinct phases throughout the process—from the onset of walking to the moment the person stops—including the initial stage, start-up stage, stable stage, and recovery stage. As shown in the figure, during the initial stage, PER for all four air supply speeds is relatively similar, remaining above 98%, indicating that the clean air layer around the nose and mouth is initially well established. Once walking begins, the PER for a 2 m/s neck-side supply drops sharply and stabilizes at around 8% after a brief period of fluctuation, highlighting the vulnerability of low-speed ventilation to dynamic disturbances. Increasing the air supply velocity enhances the system's ability to resist walking-induced airflow interference. At 3 m/s, PER during the uniform walking stage stabilizes around 46%, showing a moderate protective effect. Further increasing the supply speed to 4 m/s prevents the initial sharp drop entirely, with PER fluctuating between 91% and 94% during steady walking, demonstrating a substantial protective capability of the neck-side airflow. At 5 m/s, the lateral neck-side air supply maintains consistently high protective effectiveness throughout the walking process, showing no initial drop or subsequent impact, effectively preserving the integrity of the clean air layer and ensuring continuous respiratory protection even under sustained movement.

An analysis of the start and stop phases of walking indicates that the impact of walking on the lateral neck-side air supply is immediate and highly sensitive. When the air supply is insufficient to fully counteract the disturbance caused by walking, any change in walking state is quickly reflected in the protective performance of the neck-side airflow. Increasing the air supply speed slightly delays the cliff point at which the protective effect declines, with this delay being approximately 0.1 seconds. Simultaneously, a higher supply speed also slightly advances the time at which the protective effect begins to recover, again by about 0.1 seconds. These observations suggest that both the onset and recovery of the protective layer are closely tied to the air supply velocity, highlighting the importance of

adequate airflow in maintaining continuous respiratory protection during dynamic human movement.

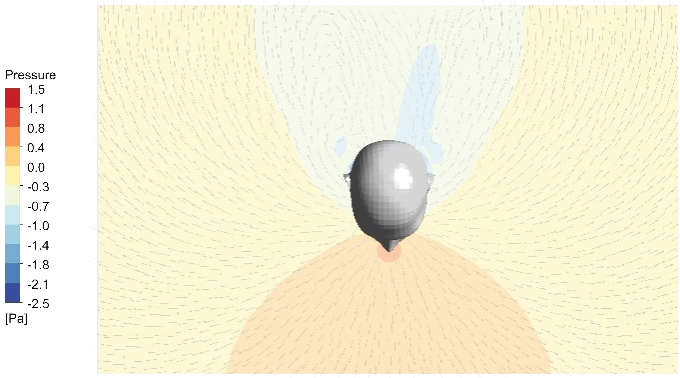

Fig.11 The pressure distribution during movement, z = 1.68m

During forward movement, the air in front of the face is compressed, forming a relatively high-pressure region, while a low-pressure zone develops behind the head, as illustrated in Fig.11. The figure shows that air pressure is particularly elevated in the region directly in front of the tip of the nose. For the neck-side ventilation system, this high-pressure zone impedes the deflection of the supplied air along the face, preventing it from converging at the nose and forming an effective clean air layer. Higher air speeds and larger airflow volumes enable the neck-side ventilation system to overcome the influence of this high-pressure region, allowing the airflow to reach the breathing zone, as confirmed by the simulations in this section. Accordingly, it can be inferred that if a person walks at a faster pace, resulting in an even higher pressure in front of the face, a correspondingly higher supply air velocity is necessary to maintain the protective effect of the neck-side airflow and ensure continuous shielding of the nose and mouth.

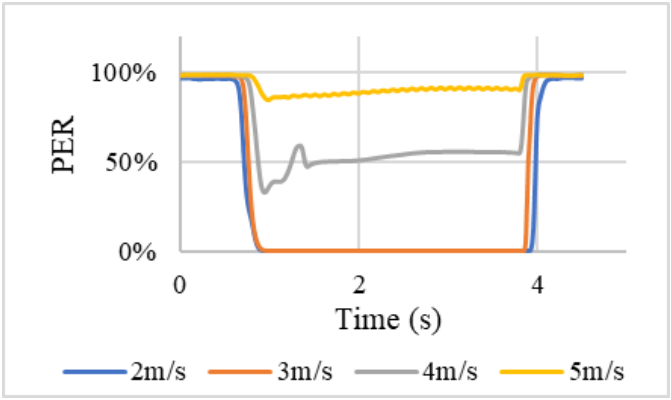

Fig.12 The PER variation of four air supply speeds under the dual interference of oncoming wind and person movement

Figure 12 illustrates the protective effect of different neck-side air supply speeds when the human body moves against a head-on wind of 0.5 m/s. Compared with the previous section, the introduction of a 0.5 m/s headwind during walking adds an additional

disturbance, causing noticeable changes in the protective performance. The stage most affected by this superimposed wind is the stable stage, where the protective effect at all supply air speeds decreases. At supply velocities of 2 m/s and 3 m/s, the neck-side airflow offers virtually no protection during this stage. With a supply speed of 4 m/s, the protection effect initially drops below 40% and then gradually recovers, ultimately stabilizing around 55%. Under walking alone, a 5 m/s supply can achieve a PER of 99%, but when subjected to the head-on wind disturbance, even this maximum supply speed is affected: after the start-up stage, the protective effect reaches 86% and slowly rises to stabilize at approximately 91%. These results clearly demonstrate that, compared with walking alone, higher supply air speeds are required to maintain effective protection when ambient head-on wind is present, emphasizing the importance of adjusting ventilation parameters to account for environmental disturbances.

Conclusion

This study introduces a neck-side ventilation approach designed to direct clean airflow from lateral inlets along the contours of the face using the Coanda effect. The airflow deflects toward the face, creating a protective clean air layer around the nose and mouth, thereby reducing human exposure to pollutants in contaminated environments. The protective performance of this ventilation system was verified through both airflow visualization experiments and CFD simulations. Building on static-condition investigations, the study further examined the effectiveness of neck-side ventilation in blocking pollutants under the combined influence of environmental wind and human movement. The mechanisms underlying the impact of these disturbances on the neck-side air supply were also analyzed. The simulation results demonstrated the following key findings:

1)Airflow visualization experiments confirmed that neck-side ventilation is effective in reducing pollutant exposure.

2)CFD simulations showed that when the roll angle is 0°, the Coanda effect fails to fully deflect and converge the air streams in front of the face. At roll angles of 15°, 30°, and 45°, the airflow deflects along the face and converges in front of it, forming a clean air layer. Roll angles of 30° and 45° were most effective, achieving a maximum PER of 75.2%.

3)The pitch angle influences PER by adjusting the convergence point of the air streams in front of the face. Pitch angles of 40° and 45° lower the convergence point, enabling the formation of a clean air layer around the nose and mouth. Increasing the pitch angle from 30° to 45° can improve PER by up to 27%, with a minimum improvement of 12.3%.

4) Under head-on wind conditions, the protective effect of neck side ventilation will be affected. However, under the conditions of head-on wind velocity of 0.5m/s and 1m/s, neck side ventilation can provide 99% PER by adjusting the supply air velocity, and it can also provide approximately 55% PER at 2.5m/s. When the user of neck ventilation moves

forward at a speed of 1m/s, the high-pressure area generated in front of the face will affect the formation of a clean air layer. To maintain a high protective effect, the air supply speed needs to be increased to 4m/s

4. Published Paper etc.
[Underline the representative researcher and collaborate researchers]
[Published papers]
1. **Zhang, W.**, **Zhang, W., & Xuan, Y**. (2025). Cognitive performance under dynamic supply air modulation: dual-objective balancing of thermal comfort and work productivity. Journal of Building Engineering, 114754.
2. **Zhang, W., Zhang, W., Xuan, Y.** Ding X. (2025). Dynamic ventilation control-induced airflow fluctuations: skin temperature response and subjective assessment in adaptive environments. Energy and Buildings, 116289.
3. **Zhang, H., Zhang, W., Xuan, Y.** Ding X. (2026). The Influence of External Interference on the Reduction of Pollutant Exposure in Neck-side Ventilation. Building and Environment (Under Review)

5. [Presentations at academic societies]
1. N/A
2.

[Published books]
1. N/A
2.

[Other]
Intellectual property rights, Homepage etc.
N/A

5. Research Group
1. Representative Researcher
Weirong ZHANG, Yingli XUAN

2. Collaborate Researchers
1. Haotian ZHANG
2. Weijia ZHANG

6. Abstract (half page)

Existing wearable respiratory devices often compromise comfort and convenient for protection. This study develops a neck-side ventilation system combining CFD simulations and experiments to address this gap. The design employs dual vents to direct airflow along facial contours via the Coanda effect, creating a protective air layer around the nose/mouth. Firstly, under the condition of no environmental disturbance, the capacity of the neck side ventilation system was verified and the parameter selection range was determined through the parameter analysis of the roll angle (0°-45°), pitch angle (30°-45°) and airspeed (1–2 m/s). Then, a 45° roll angle and a 40° pitch angle were selected to verify the anti-disturbance ability of the neck side ventilation system in the scenarios of frontal wind and human movement. The results show that the protection effect is better when the roll angle is greater than 30° and the pitch angle is greater than 40°. Under the appropriate air supply angle, the cleaning effect of the neck side ventilation system under disturbed conditions can reach over 90% of that under static conditions, verifying its anti-disturbance ability. This work demonstrates the feasibility of the neck side ventilation system as a low-resistance alternative to traditional masks in polluted environments.